NASA Technical Memorandum 103782

Elastic Response of [001]-Oriented PWA 1480 Single Crystal—The Influence of Secondary Orientation

Sreeramesh Kalluri and Ali Abdul-Aziz
Sverdrup Technology, Inc.
Lewis Research Center Group
Brook Park, Ohio

and

Michael A. McGaw
National Aeronautics and Space Administration
Lewis Research Center
Cleveland, Ohio

Prepared for the
1991 Aerospace Atlantic Meeting
sponsored by the Society of Automotive Engineers
Dayton, Ohio, April 23–26, 1991

Elastic Response of [001]-Oriented PWA 1480 Single Crystal - The Influence of Secondary Orientation

Sreeramesh Kalluri and Ali Abdul-Aziz
Sverdrup Technology, Inc.,
NASA Lewis Research Center Group
Cleveland, Ohio 44135

and

Michael A. McGaw
NASA Lewis Research Center
Cleveland, Ohio 44135

Abstract

The influence of secondary orientation on the elastic response of a [001]-oriented nickel-base single-crystal superalloy, PWA 1480, was investigated under mechanical, thermal, and combined thermal and mechanical loading conditions by applying finite element techniques. Elastic stress analyses were performed with a commercially available finite element code. Secondary orientation of the single-crystal superalloy was offset with respect to the global coordinate system in increments from 0° to 90° and stresses developed within the single crystal were determined for each loading condition. The results indicated that the stresses were strongly influenced by the angular offset between the secondary crystal orientation and the global coordinate system. The degree of influence was found to vary with the type of loading condition (mechanical, thermal, or combined) imposed on the single-crystal superalloy.

Introduction

Single crystal (SC) superalloys were identified as potential blade materials that warranted further development for advanced liquid propellant rocket engine turbopumps by Chandler (1). After subsequent development, materials scientists evaluated the mechanical properties of several single crystal superalloys (2,3) to find a suitable candidate replacement blade material for the turbopumps of the Space Shuttle Main Engine (SSME) and advanced rocket engines. A well characterized, nickel-base cubic single crystal superalloy, PWA 1480, was selected by Pratt & Whitney as the blade material for the Alternate Turbopump Development (ATD) program for the SSME.

Turbine blades of nickel-base single crystal superalloys (including PWA 1480) are directionally solidified along the low modulus [001] crystallographic direction to enhance thermal fatigue resistance. The directional solidification process usually generates a secondary crystallographic direction, [010] that is randomly oriented with respect to fixed geometric axes in the turbine blade. However, orientation of the secondary crystallographic direction can be controlled by using a seed crystal during solidification (4). Since single crystals exhibit anisotropic elastic behavior, the stress-strain response and dynamic characteristics of a turbine blade that is directionally cast along the [001] crystal orientation tend to vary with the orientation of the secondary crystallographic direction within the blade (5-6).

The main objective of this study was to determine the influence of secondary orientation on the elastic response of [001]-oriented, single crystal PWA 1480 under mechanical, thermal, and combined thermal and mechanical loading conditions by applying finite element stress analyses. A parametric study was conducted in which the secondary orientation angle was varied in increments of 10° from 0° to 90° for each loading condition. The stresses developed within the single crystal PWA 1480 superalloy for all the cases of the parametric study are presented.

The turbine blade of a rocket engine turbopump is schematically represented in Fig. 1. This is a hollow SC PWA 1480 turbine blade that is directionally cast such that the [001] crystallographic direction (primary orientation) is parallel to the span of the blade. In this particular design the hollow core extends below the platform into the shank region. In Fig. 1, XYZ is the global coordinate system, with Z-axis along the span of the blade, Y-axis along the chord of the blade, and X-axis along the thickness of the blade.

In a cryogenic liquid propellant rocket engine turbopump, the blade attachment region may be actively cooled. Since the turbine blade airfoil is exposed to the hot gas flow path, thermal gradients are induced both along the span of the blade as well as through the thickness, for the

full length of the hollow core. These gradients may be especially severe through the thickness (of the order of 875 °C/cm), while being milder along the span. These gradients are substantially higher than those in typical aircraft gas turbine blades. To examine the role which the secondary crystal orientation may play in such cases, an analysis of a square plate subjected to similar loadings will be employed (Fig. 1).

A square plate with the dimensions of 25.4 by 25.4 by 3.2 mm was selected for the parametric finite element stress analyses. The crystal ($X_cY_cZ_c$) and global (XYZ) coordinate systems for the plate are shown in Fig. 1. The global coordinate system is obtained by rotating the crystal coordinate system about the Z_c-axis by an angle of θ. Since the axes Z and Z_c are both oriented along the [001] crystallographic direction, the angle θ between the crystal and global coordinate systems represents the orientation of the secondary crystallographic direction. The matrix of direction cosines that relates the global coordinate system to the crystal coordinate system (Fig. 1) is as follows:

$$\begin{pmatrix} x \\ y \\ z \end{pmatrix} = \begin{bmatrix} \cos\theta & \sin\theta & 0 \\ -\sin\theta & \cos\theta & 0 \\ 0 & 0 & 1 \end{bmatrix} \begin{pmatrix} x_c \\ y_c \\ z_c \end{pmatrix} \qquad (1)$$

ELASTIC STIFFNESS COEFFICIENTS

Three independent elastic stiffness coefficients (C_{11}, C_{12} and C_{44}; Eq. (2)) are required to describe the elastic behavior of a cubic single crystal such as SC PWA 1480 within the crystallographic coordinate system (7). To describe the elastic behavior in the global coordinate system the stiffness tensor must be transformed from the crystal coordinate system to the global coordinate system (Fig. 1) according to the law of transformation of fourth rank tensors. Lieberman and Zirinsky (8) developed a simplified method for transforming the stiffness coefficients of single crystals between two coordinate systems that are related by a matrix of direction cosines (Eq. (1)). Their method was used together with Eq. (1) to obtain the elastic stiffness coefficients of a cubic single crystal in the global coordinate system. The stiffness matrix of the cubic single crystal within the global coordinate system and its relationship to the engineering stresses and engineering strains is as follows:

$$\begin{pmatrix} \sigma_{xx} \\ \sigma_{yy} \\ \sigma_{zz} \\ \tau_{yz} \\ \tau_{zx} \\ \tau_{xy} \end{pmatrix} = \begin{bmatrix} D_{11} & D_{12} & C_{12} & 0 & 0 & D_{16} \\ D_{12} & D_{11} & C_{12} & 0 & 0 & D_{26} \\ C_{12} & C_{12} & C_{11} & 0 & 0 & 0 \\ 0 & 0 & 0 & C_{44} & 0 & 0 \\ 0 & 0 & 0 & 0 & C_{44} & 0 \\ D_{16} & D_{26} & 0 & 0 & 0 & D_{66} \end{bmatrix} \begin{pmatrix} \varepsilon_{xx} \\ \varepsilon_{yy} \\ \varepsilon_{zz} \\ \gamma_{yz} \\ \gamma_{zx} \\ \gamma_{xy} \end{pmatrix} \qquad (2)$$

where,

$$D_{11} = C_{11} - 2(C_{11} - C_{12} - 2C_{44}) \times \sin^2\theta \cos^2\theta \qquad (3)$$

$$D_{12} = C_{12} + 2(C_{11} - C_{12} - 2C_{44}) \times \sin^2\theta \cos^2\theta \qquad (4)$$

$$D_{16} = (C_{11} - C_{12} - 2C_{44})(\sin^3\theta\cos\theta - \sin\theta\cos^3\theta) \qquad (5)$$

$$D_{26} = -D_{16} \qquad (6)$$

$$D_{66} = C_{44} + 2(C_{11} - C_{12} - 2C_{44}) \times \sin^2\theta \cos^2\theta \qquad (7)$$

In Eq. (2), σ_{xx}, σ_{yy}, σ_{zz} and τ_{yz}, τ_{zx}, τ_{xy} are the engineering normal and shear stresses, respectively, and ε_{xx}, ε_{yy}, ε_{zz} and γ_{yz}, γ_{zx}, γ_{xy} are the engineering normal and shear strains, respectively. Thus, Eqs. (2) to (7) define the stiffness matrix in a global coordinate system (XYZ) that is offset by an (arbitrary) angle θ to the crystal coordinate system ($X_cY_cZ_c$; Fig. 1).

The three independent elastic stiffness coefficients (applicable within the crystal coordinate system) for SC PWA 1480 at various temperatures are listed in Table 1. These coefficients were determined by the Engineering Division of Pratt & Whitney, United Technologies Corporation under the NASA Lewis Research Center contract NAS3-23939. The variations of stiffness coefficients D_{11}, D_{12}, D_{16}, D_{26} and D_{66} with the secondary orientation angle θ, determined from Eqs. (2) to (7) for SC PWA 1480 at 38 °C, are shown in Fig. 2. It is evident from this figure that the variation in the elastic stiffness coefficients has a periodicity of 90° in θ, and therefore, a range of 0 to 90° was selected for the secondary orientation angle in the parametric study.

FINITE ELEMENT ANALYSES

Elastic stress analyses were conducted on the plate model shown in Fig. 3 by using the MARC finite element structural analysis code (9). The finite element model of the plate contained a total of 500 isoparametric eight-noded solid elements with ten elements along the side and five elements through the thickness of the plate. The boundary conditions used were as follows: (1) the node at D was fixed in X, Y, and Z directions, (2) nodes along the edge AD were fixed in Y and Z directions, (3) nodes along the edge DC were fixed in X and Z directions and (4) nodes along edges AB and BC were fixed in the Z direction. All boundary conditions were enforced by specifying the fixed boundary option of the MARC code. A total of five different loading cases were considered in this study. In these cases mechanical, thermal and combined mechanical and thermal loads were applied separately to the model. The previously described boundary conditions were employed in all five loading cases.

The first loading case involved a distributed mechanical load of 137.9 MPa along the Z-direction (Fig. 4(a)). In the second and third loading cases thermal gradients were imposed along the Z- and X-direction, respectively (Figs. 4(b) and (c)). Imposition of thermal gradients along the Z and X directions was an attempt to simulate the thermal gradients that occur along the span and through the thickness of the actual turbine blade. Finally, the fourth and fifth loading cases were obtained by combining the first loading case with the second and third loading cases, respectively.

The physical properties of SC PWA 1480 including mean coefficient of thermal expansion, thermal conductivity and specific heat were obtained from Ref. 10. For the loading cases involving thermal gradients, thermal boundary conditions represented by the temperatures in Fig. 4 were applied to the finite element model considered. These thermal boundary conditions may be representative of cryogenic rocket engine turbomachinery turbine blade applications. Thermal boundary conditions were introduced into the finite element code enforcing the assigned temperatures to the specific faces of the plate in Fig. 4, while insulating all other faces. Thermal gradients shown in Fig. 5 were used in the second and third loading cases. These data represent temperatures at the centroids of the elements. The thermal output feature of MARC code was used to generate the input subsequent stress analysis.

For each loading case in the parametric study, the secondary orientation angle θ was varied from 0° to 90° in increments of 10°. In addition, all loading cases were studied for θ = 45° to obtain the data at the symmetric location (Fig. 2). The stiffness matrices for the various secondary orientations were incorporated in the finite element analyses by programming Eq. (2) in the MARC user's subroutine HOOKLW (9). Variations in the physical and elastic properties of the material with temperature were accounted for in the analyses.

The variations in the different components of stress with secondary crystal orientation angle θ were documented for three elements shown in Fig. 3. These elements were selected to capture the extreme as well as reference stress locations for the five different loading cases considered in this study. For example, under the second loading case in which a thermal gradient was imposed along the Z-direction (Fig. 4(b)), extreme thermal stresses could be generated in faces ABCD and EFGH. Hence, the selection of element 295 (Fig. 3) which was near surface EFGH for this loading case. Similar reasoning was used in selecting element 445 (Fig. 3), for the third loading case in which a thermal gradient was imposed along the X-direction. Finally, a centrally located, element 245 (Fig. 3) was selected for the first loading case in which only the mechanical loading was imposed. Another consideration that led to the choice of these specific locations was mitigation of the constraint effects on the stresses generated within the elements.

For the five loading cases considered in this study, the values of the six stress components at the centroid of the selected elements are listed in Table 3 for a secondary orientation angle of θ = 0°. In all loading cases the stresses developed within the three selected elements were well within the elastic regime of SC PWA 1480. In loading Case 1, which involved only mechanical loading, values of the six stress components in the three selected elements were very similar. However, in loading Cases 2 and 3 which involved thermal gradients along the Z- and X-axis, respectively, elements 295 (near the hot side of a thermal gradient along Z-axis) and 445 (near the cold side of a thermal gradient along X-axis) were subjected to large normal compressive and tensile stresses, respectively, compared to the normal stresses in element 245 which was nearly at the center of the mesh. The magnitudes of the tensile normal stresses of element 445 in loading Case 3 were larger than the magnitudes of compressive normal stresses in

element 295 under loading Case 2 because the square plate was subjected to a more severe thermal gradient along the thickness (X-axis) than along the length (Z-axis). Finally, in loading Cases 4 and 5 which involved both mechanical and thermal loading, the stresses developed within the selected elements were very nearly equal to those expected from the superposition of stresses developed in the individual mechanical and thermal loadings (loading Case 1 with loading Cases 2 and 3, respectively). These results are in agreement with the principle of superposition for the linear elastic analysis.

The influence of secondary orientation on the stresses developed within the selected elements are shown in Figs. 6 to 8. For each element and loading case, the individual stress components at a given secondary orientation angle θ were normalized with the corresponding stress components obtained for $\theta = 0°$, i.e. $(\sigma_{xx})_\theta/(\sigma_{xx})_{\theta=0}$, $(\sigma_{yy})_\theta/(\sigma_{yy})_{\theta=0}$, and $(\tau_{xy})_\theta/(\tau_{xy})_{\theta=0}$ and so on. The individual as well as normalized stress components were then plotted against the secondary orientation angle θ for each element and loading condition. If there was no influence of secondary orientation on the elastic response of SC PWA 1480, then all six normalized stress components should remain at a fixed value of unity as θ is varied from 0° to 90°. Any deviation from unity is an indication that the elastic response of PWA 1480 SC is affected by the secondary orientation angle θ. The influence of secondary orientation on individual and normalized stress components under imposed mechanical loading (Case 1) is shown in Fig. 6 for the three selected elements. The variation of individual and normalized stress components with secondary orientation angle θ are shown in Figs. 7 and 8 for thermal loads (loading Cases 2 and 3) and combined thermal and mechanical loads (loading Cases 4 and 5), respectively.

The influence of the secondary orientation angle on both the individual and normalized stress components was dictated by the type (mechanical or thermal or combined) of loading imposed on the SC PWA 1480 square plate. For example, no significant influence of secondary orientation was observed for the individual stress components under mechanical loading (Fig. 6). However, in cases involving thermal gradients along X- and Z-axis the individual normal stress components exhibited significantly larger influence of secondary orientation than the individual shear stresses (Figs. 7 and 8). The normalized stress components exhibited a substantial dependence on the secondary orientation angle, θ under all five loading cases. In all of the loading cases except those involving thermal gradient along the X-axis, largest influence of secondary orientation was observed for the normalized stress component $(\tau_{xy})_\theta/(\tau_{xy})_{\theta=0}$. For the cases involving thermal gradient along the X-axis the normalized components $(\sigma_{xx})_\theta/(\sigma_{xx})_{\theta=0}$ and $(\tau_{xy})_\theta/(\tau_{xy})_{\theta=0}$ exhibited about the same order of variation with the secondary orientation angle, θ.

DISCUSSION

In this study, the elastic stress components were normalized to determine the influence of secondary orientation angle θ, under different loading conditions. In Figs. 6 to 8 the normalized stress components indicate that, on a relative basis, all six components of stress are influenced by the secondary orientation angle, θ. However, the importance of secondary orientation effects cannot be evaluated by consideration of the variation in the normalized stress components (with θ) alone. The magnitudes of the individual components must also be taken into consideration for accurate assessment of the influence of secondary orientation. For example, one normalized stress component, $(\tau_{xy})_\theta/(\tau_{xy})_{\theta=0}$, exhibited a range as large as ±166 in element 295 under loading Case 2, in which thermal loading was imposed along the Z-axis (Fig. 7(a)(ii)). However, it is clear from Table 3 that the value of τ_{xy} at $\theta = 0°$ is only 0.005 Mpa. For this loading condition, multiplying this stress component by a factor of 166 yields 0.830 MPa, a relatively small value compared to the other normal components of stress within this element (Fig. 7(a)(i)). By comparison, the normalized stress component $(\sigma_{yy})_\theta/(\sigma_{yy})_{\theta=0}$ increased only from 1.0 to 1.4 as θ was increased from 0° to 90° under thermal loading along the X-axis (Fig. 7(b)(ii)). However, this represented an increase in σ_{yy} from 204.2 MPa at $\theta = 0°$ to 286.3 MPa at $\theta = 45°$ (Fig. 7(b)(ii)). Thus, the variations in the normalized stress components with θ, while indicative of the influence of secondary orientation on the elastic response of SC PWA 1480, alone are not sufficient to assess the importance of secondary orientation effects. The variation of actual magnitudes of the individual components of stress also must be considered to determine the quantitative significance of the secondary orientation effects.

Among the mechanical, thermal and combined loading cases considered in this study, the case of a thermal gradient along the X-axis (through the thickness of the square plate) produced large stresses (Table 3; In Case 3, element 445 is under biaxial tension). This is due to the fact that the thermal gradient through the thickness of the plate is more severe than the thermal gradient along the length of the square plate (Fig. 5). In loading case 5, the mechanical load which was superimposed on the thermal load of Case 3, nearly doubled the σ_{zz} component of stress within the square plate (Table 3; Case 5, element 445).

The state of maximum biaxial tension occurred for loading Case 5 at a secondary orientation angle $\theta = 45°$ (Table 3, element 445 and Fig. 8(b)(i)). This is to be expected because in this instance the stiffness coefficient D_{11} (which reaches a maximum at $\theta = 45°$, Fig. 2) is coupled with a steep thermal gradient through the thickness of the square plate and a mechanical load along the Z-axis. Thus, large

thermal gradients perpendicular to the primary orientation [001] of the turbine blade may be expected to produce very high stresses, if they occur near the secondary orientation of $\theta = 45°$. However, these stresses can be minimized by controlling the secondary orientation so that thermal gradients perpendicular to [001] occur near $\theta = 0°$.

Some normalized stress components shown in Figs. 6 to 8 exhibit a lack of symmetry about the secondary orientation angle, $\theta = 45°$. For example, the normalized stress component $(\sigma_{xx})_\theta/(\sigma_{xx})_\phi$ is not symmetric about $\theta = 45°$. Similar behavior is also exhibited by the normalized stress components, $(\tau_{xy})_\theta/(\tau_{xy})_\phi$ and $(\tau_{yz})_\theta/(\tau_{yz})_\phi$ in Fig. 6(c)(ii) and by $(\sigma_{xx})_\theta/(\sigma_{xx})_\phi$, $(\tau_{xy})_\theta/(\tau_{xy})_\phi$, and $(\tau_{yz})_\theta/(\tau_{yz})_\phi$ in Fig. 8(b)(ii). The main reason for lack of symmetry about $\theta = 45°$ is the coupling between σ_{xx} and σ_{yy} and γ_{xy} as well as between τ_{xy} and ε_{xx} and ε_{yy} in the single crystal stiffness matrix (Eq. (2)). The coupling elastic coefficients D_{16} and D_{26} change sign about $\theta = 45°$ (Fig. 2) which creates a lack of symmetry in the stress components. A small amount of observed lack of symmetry may also have been caused by numerical round off errors. This may especially be the reason for the observed asymmetry in $(\tau_{yz})_\theta/(\tau_{yz})_\phi$, because τ_{yz} has no coupling terms in the single crystal stiffness matrix.

In this study the influence of secondary orientation was studied under purely elastic conditions and steady state thermal gradients. In actual service, turbine blades are subjected to severe thermal transients due to start up and shutdown, which can produce localized plasticity and creep in the turbine blades. The influence of secondary orientation on the stresses produced within the actual blade under conditions of plasticity and creep will be different from the influence determined under fully elastic conditions. To determine the influence of secondary orientation on the stresses developed within the turbine blades, nonlinear, transient thermal structural analyses must be conducted with appropriate boundary conditions.

CONCLUSIONS

A parametric study was conducted with elastic finite element analyses to determine the influence of secondary orientation angle on the elastic behavior of a [001]-oriented nickel-base single crystal superalloy, PWA 1480 under mechanical, thermal and combined mechanical and thermal loads. The secondary orientation angle was varied from 0° to 90° and the stresses developed within a square plate of SC PWA 1480 under different loading conditions were computed. The following conclusions were drawn from the parametric study.

1. Under the loading conditions studied, the normalized stress components showed a substantial variation with the secondary orientation angle. However, the normalized stress components should be considered along with the magnitudes of the individual stress components to determine the significance of secondary orientation in engineering design.

2. The type of loading (mechanical, thermal, or combined) imposed on the square plate dictated the variation in the individual stress components with the secondary orientation angle.

3. For the same temperature boundary conditions, thermal gradients through the thickness of the square plate produced higher stresses than thermal gradients along the length (primary orientation of [001]) of the square plate. This was due to a higher thermal gradient through the thickness of the plate. If it is required to impose thermal gradients perpendicular to the primary [001] orientation, a secondary orientation of 0° tends to minimize the thermal stresses developed within the plate, whereas a secondary orientation of 45° tends to produce much larger thermal stresses.

REFERENCES

1. Chandler, W.T., "Materials for Advanced Rocket Engine Turbopump Turbine Blades," Advanced High Pressure O_2/H_2 Technology, S.F. Morea and S.T. Wu, eds., NASA CP-2372, 1985, pp. 110-132.

2. Dreshfield, R.L., and Parr, R.A., "Application of Single Crystal Superalloys for Earth-to-Orbit Propulsion Systems," AIAA Paper 87-1976, 1987. (Also, NASA TM-89877.)

3. Fritzemeier, L.G., "Advanced Single Crystal for SSME Turbopumps," RI/RD 88-273, Rockwell International Corp., NASA CR-182244, 1989, pp. 1-44.

4. Duhl, D.N., "Single Crystal Superalloys," Superalloys, Supercomposites and Superceramics, J.K. Tien and T. Caulfield, eds., Academic Press, Inc., 1989, pp. 149-182.

5. Bowen, K., Nagy, P., and Parr, R. A., "The Evaluation of Single Crystal Superalloys for Turbopump Blades in the SSME," AIAA Paper 86-1477, 1986.

6. Abdul-Aziz, A., August, R., and Nagpal, V., "Design Considerations for a Space Shuttle Main Engine (SSME) Turbine Blade Made of Single Crystal Material," AIAA Paper 89-2149, 1989.

7. Nye, J.F., Physical Properties of Crystals: Their Representation by Tensors and Matrices, Calendron Press, Oxford, 1957, pp. 131-149.

8. Lieberman, D.S., and Zirinsky, S., "A Simplified Calculation for the Elastic Constants of Arbitrarily Oriented Single Crystals," Acta Cryst., vol. 9, 1956, pp. 431-436.

9. MARC General Purpose Finite Element Analysis Program, Vol. A: User Information Manual; Vol. B: Marc Element Library; Vol. F: Theoretical Manual. MARC Analysis Corp., Palo Alto, CA, 1988.

10. Swanson, G.A., Linsak, I., Nissley, D.M., Norris, P.P., Meyer, T.G., and Walker, K.P., "Life Prediction and Constitutive Models for Engine Hot Section Anisotropic Materials," PWA-5968-47, Pratt and Whitney Aircraft Group, NASA CR-179594, 1987. (Avail. NTIS, AD-A173875.)

TABLE 1.- INDEPENDENT ELASTIC STIFFNESS COEFFICIENTS FOR SC PWA 1480

Temperature, °C	C_{11}, GPa	C_{12}, GPa	C_{44}, GPa
-18	252	163	131
38	250	163	129
93	248	161	128
149	246	160	126
204	244	159	124
260	242	158	123
316	240	157	121
371	238	157	119
427	235	156	117
482	233	154	115
538	230	154	113
593	228	152	111
649	225	152	109
704	223	151	107
760	219	150	105
816	217	150	102
871	213	149	100
927	210	148	97
982	206	146	95
1038	201	145	92
1093	197	143	88
1149	192	143	85
1204	186	142	81

TABLE 2. - PHYSICAL PROPERTIES OF SC PWA 1480

[From Ref. (9).]

Temperature, °C	Thermal coefficient of expansion, α, m/m/°C	Thermal conductivity, k, W/m °C	Specific heat, c, kJ/kg °C
93	0.0000107	9.2	0.406
204	.0000111	10.8	.440
316	.0000115	12.4	.465
427	.0000119	13.7	.477
538	.0000124	15.3	.481
649	.0000129	16.9	.490
760	.0000134	18.5	.511
871	.0000140	20.0	.569
982	.0000147	21.5	.687
1093	.0000157	22.8	.917

TABLE 3. - STRESSES DEVELOPED IN SINGLE CRYSTAL PWA 1480 PLATE UNDER MECHANICAL, THERMAL AND COMBINED LOADING CASES SECONDARY ORIENTATION ANGLE, θ = 0°

Case	Type of loading	Element	σ_{xx}, MPa	σ_{yy}, MPa	σ_{zz}, MPa	τ_{xy}, MPa	τ_{yz}, MPa	τ_{zx}, MPa
1	Mechanical (Z-axis)	245	0.655	1.310	136.9	0.001	0.316	−0.047
		295	.012	.053	137.9	.001	−.003	−.006
		445	-.090	1.234	136.6	.005	.385	-.182
2	Thermal (Z-axis)	245	.043	−15.78	19.98	-0.017	-5.475	-.296
		295	−19.44	−20.34	-1.88	.005	.043	−0.034
3	Thermal (X-axis)	245	.034	3.020	6.847	1.496	−.270	−12.41
		445	.993	204.2	130.0	1.214	15.56	-3.744
4	Mechanical and thermal (Z-axis)	245	.697	-14.47	156.9	.018	-5.157	-.343
		295	−19.43	−20.29	136.0	.006	.040	−.041
5	Mechanical (Z-axis) and thermal (X-axis)	245	.687	4.330	143.7	1.496	.046	12.46
		445	.903	205.4	266.4	1.220	15.95	-3.923

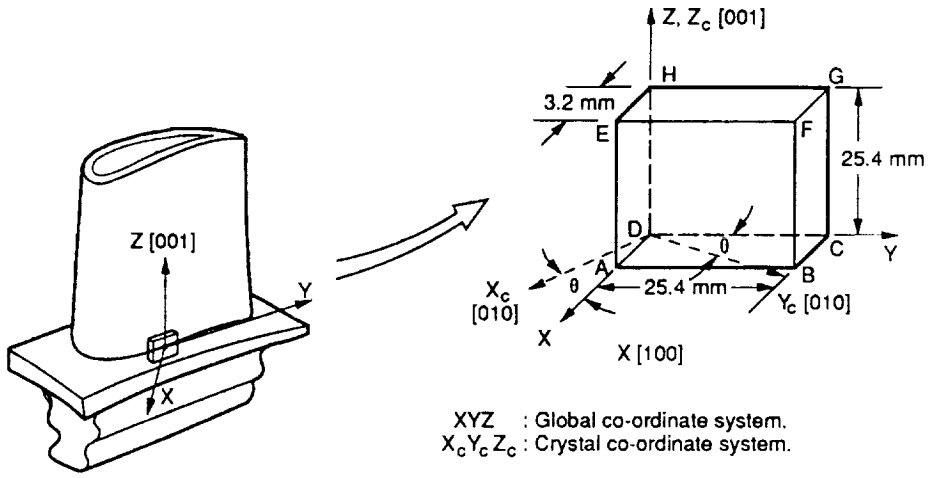

Figure 1.—Schematics of SSME turbine blade and the square plate considered for the analysis.

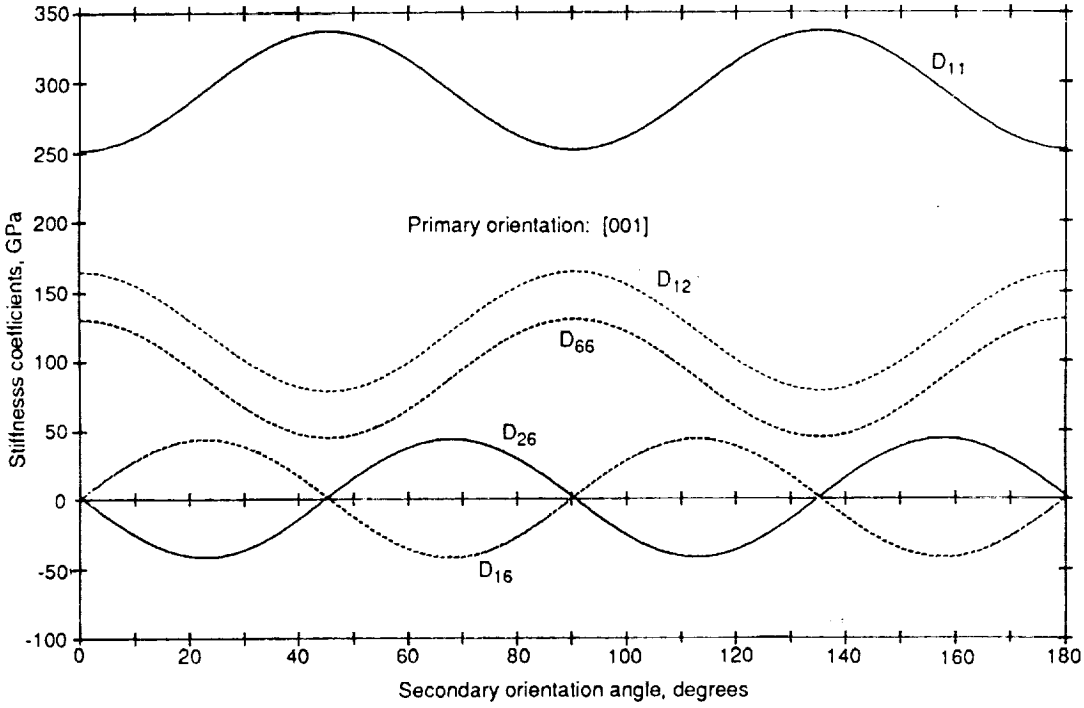

Figure 2.–Variation of elastic stiffness coefficients of SC PWA 1480 with the secondary orientation angle θ.

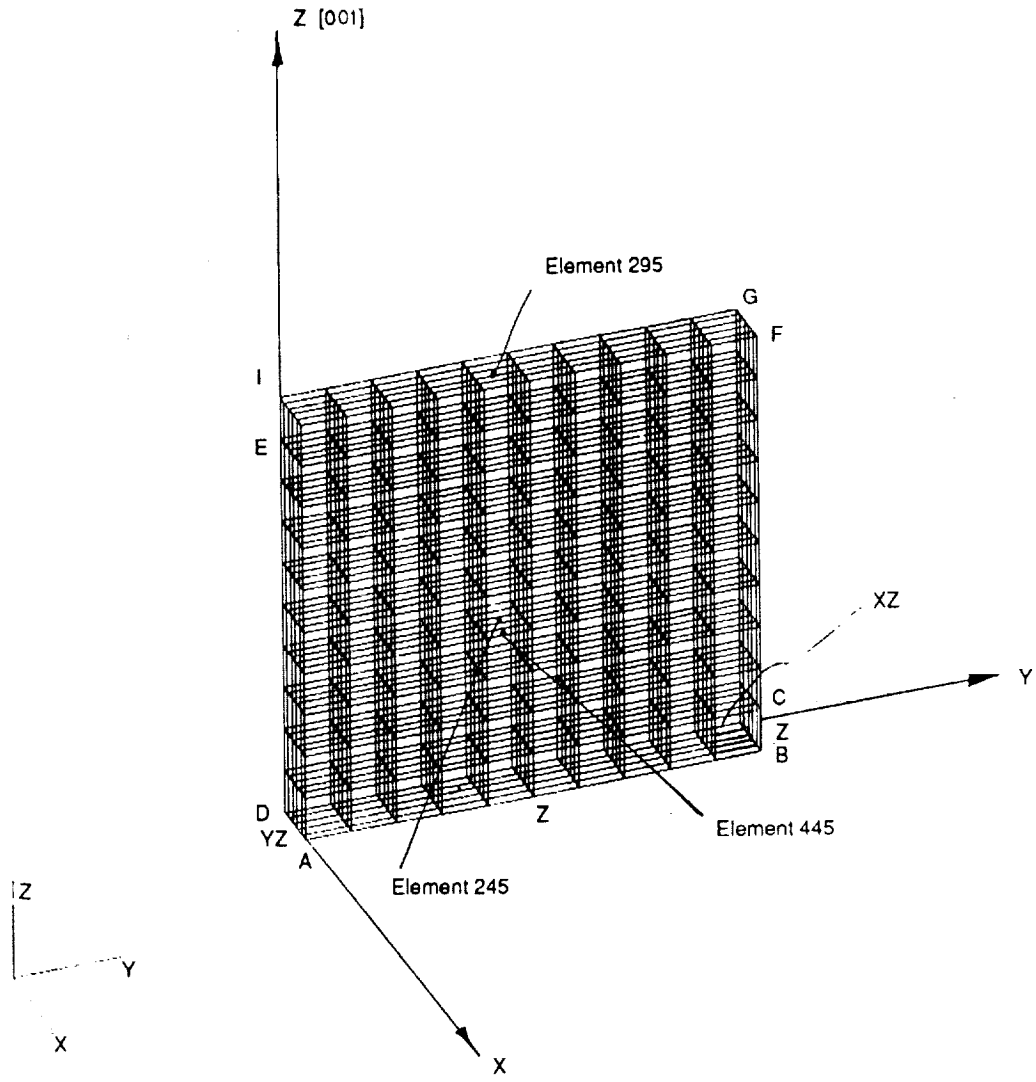

Figure 3.–Finite element mesh of the square plate.

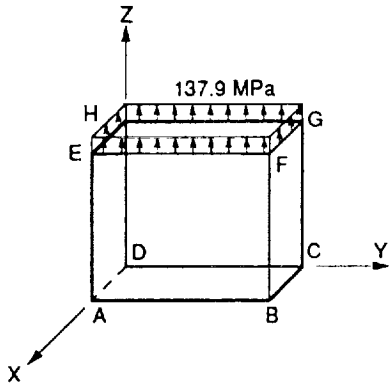

(a) Distributed mechanical load along Z-axis.

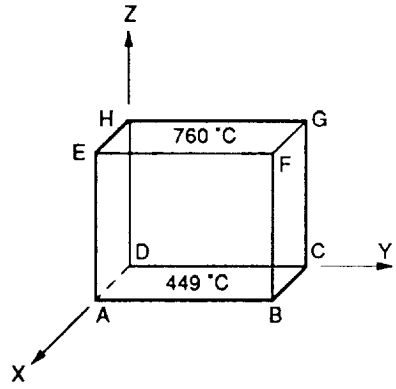

(b) Thermal gradient along Z-axis.

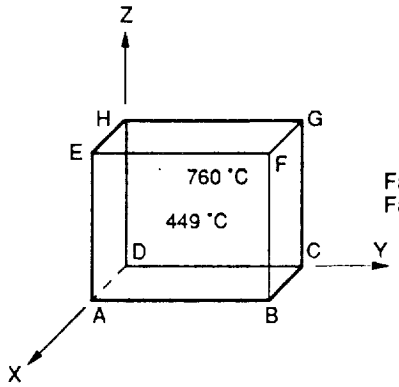

Face ABFE at 449 °C
Face DCGH at 760 °C

(c) Thermal gradient along X-axis.

Figure 4.–Loading cases imposed on the square plate.

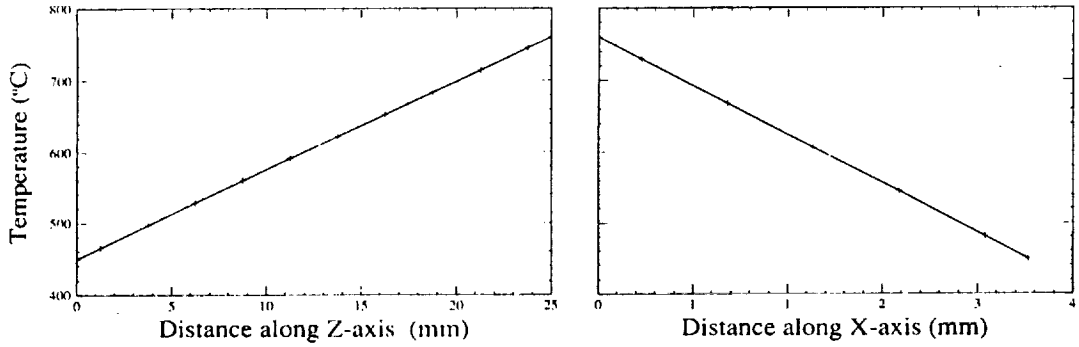

(a) Along the height of the square plate (Z–axis). (b) Through the thickness of the square plate (X–axis).

Figure 5.–Temperature distributions calculated from the heat transfer analyses.

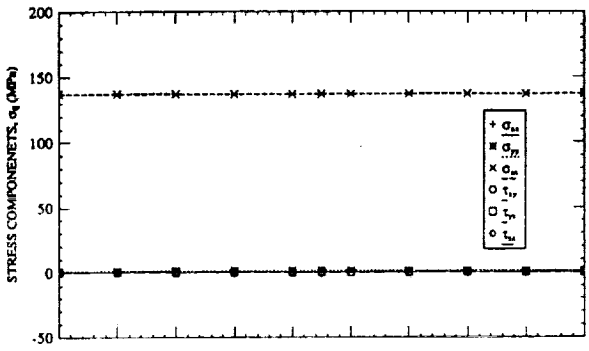

(i) Individual stress components.

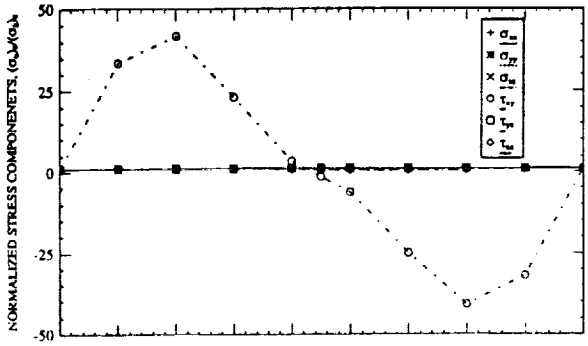

(ii) Normalized stress components.

(a) Element 245.

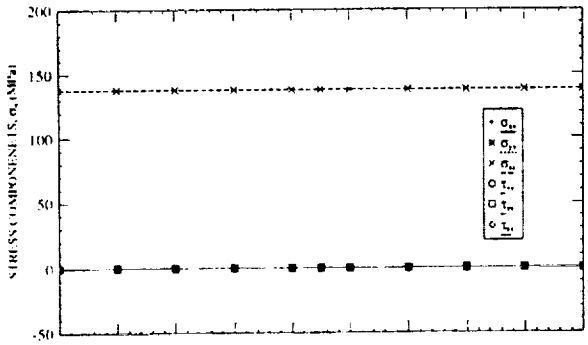

(i) Individual stress components.

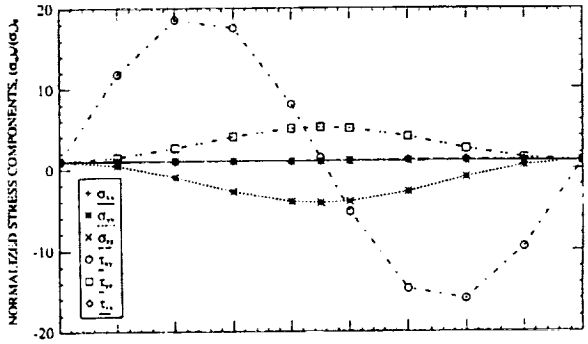

(ii) Normalized stress components.

(b) Element 295.

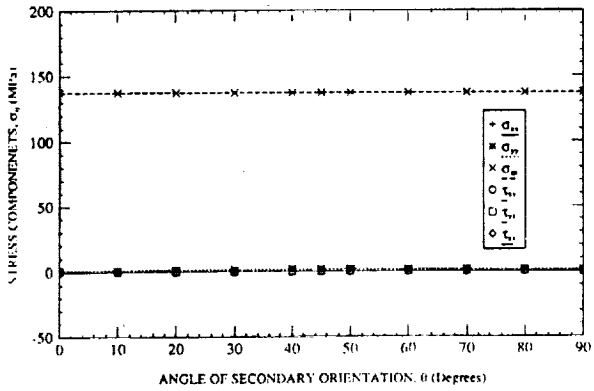

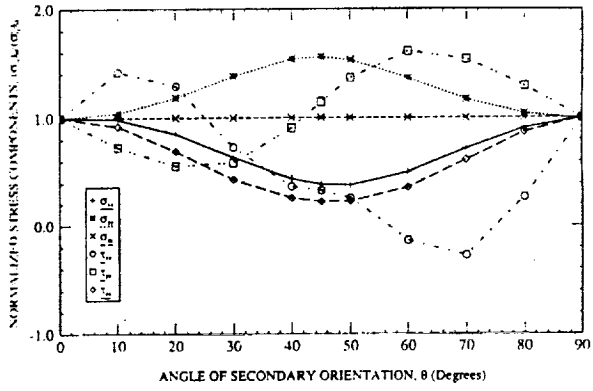

(i) Individual stress components. (ii) Normalized stress components.

(c) Element 445.

Figure 6.–Influence of secondary orientation θ on individual and normalized stress components under imposed mechanical loading.

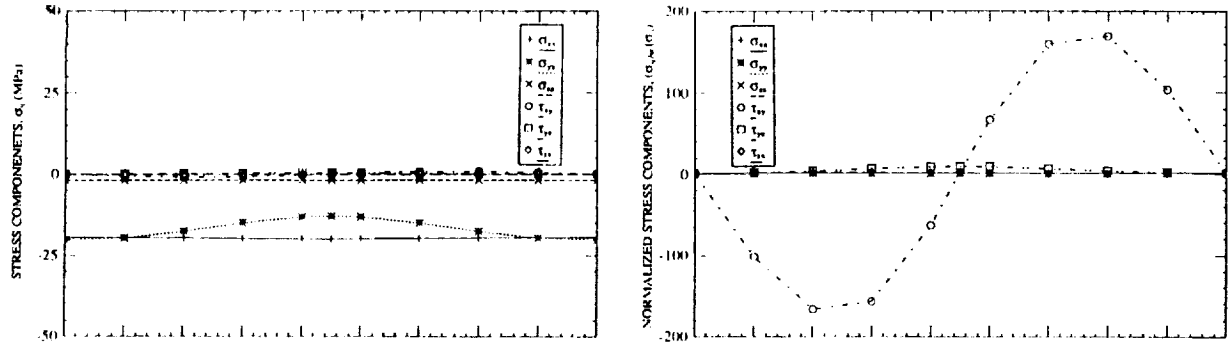

(i) Individual stress components. (ii) Normalized stress components.

(a) Thermal gradient along Z-axis; Element 295.

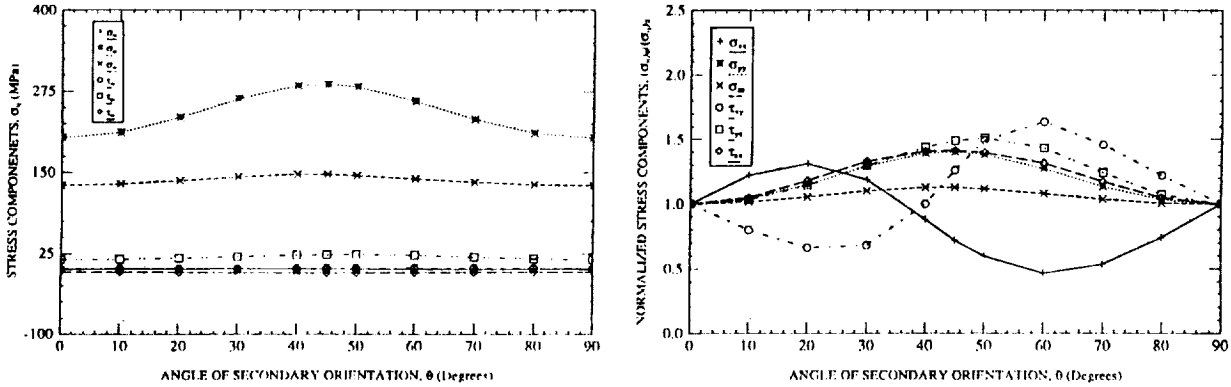

(i) Individual stress components. (ii) Normalized stress components.

(b) Thermal gradient along X-axis; Element 445.

Figure 7.–Variation of normalized stress components with secondary orientation angle θ for thermal loads.

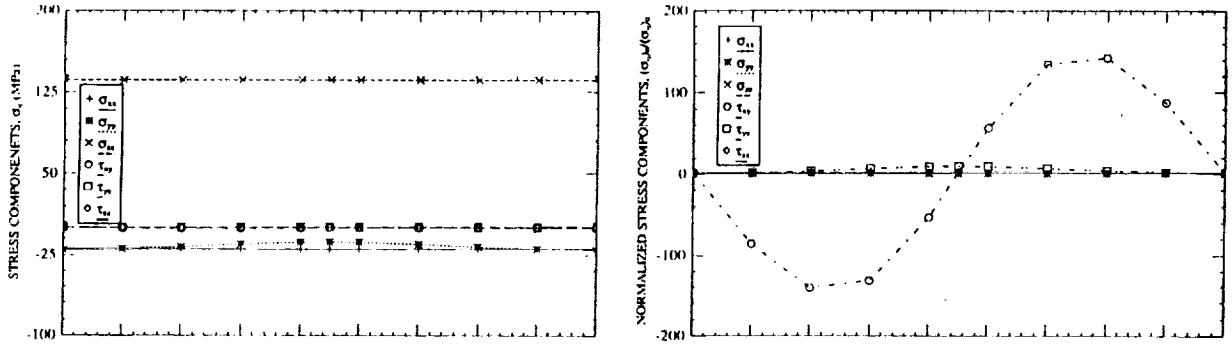

(i) Individual stress components. (ii) Normalized stress components.

(a) Thermal gradient along Z-axis; Element 295.

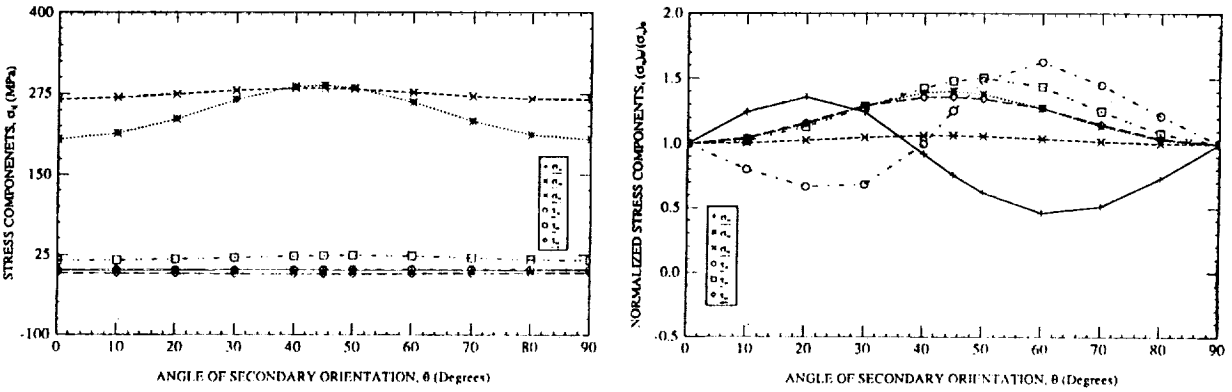

(i) Individual stress components. (ii) Normalized stress components.

(b)Thermal gradient along X-axis; Element 445.

Figure 8.–Variation of normalized stress components with secondary orientation angle θ for combined mechanical and thermal loads.

NASA
National Aeronautics and Space Administration

Report Documentation Page

1. Report No.	2. Government Accession No.	3. Recipient's Catalog No.
NASA TM-103782		

4. Title and Subtitle

Elastic Response of [001]-Oriented PWA 1480 Single Crystal—The Influence of Secondary Orientation

5. Report Date

6. Performing Organization Code

7. Author(s)

Sreeramesh Kalluri, Ali Abdul-Aziz, and Michael A. McGaw

8. Performing Organization Report No.
E-6057

10. Work Unit No.
553-13-00

9. Performing Organization Name and Address

National Aeronautics and Space Administration
Lewis Research Center
Cleveland, Ohio 44135-3191

11. Contract or Grant No.

13. Type of Report and Period Covered
Technical Memorandum

12. Sponsoring Agency Name and Address

National Aeronautics and Space Administration
Washington, D.C. 20546-0001

14. Sponsoring Agency Code

15. Supplementary Notes

Prepared for the 1991 Aerospace Atlantic Meeting sponsored by the Society of Automotive Engineers, Dayton, Ohio, April 23-26, 1991. Sreeramesh Kalluri and Ali Abdul-Aziz, Sverdrup Technology, Inc., Lewis Research Center Group, 2001 Aerospace Parkway, Brook Park, Ohio 44142 (work funded by NASA Contract NAS3-25266). Michael A. McGaw, NASA Lewis Research Center, (216) 433-3308.

16. Abstract

The influence of secondary orientation on the elastic response of a [001]-oriented nickel-base single-crystal superalloy, PWA 1480, was investigated under mechanical loading conditions by applying finite element techniques. Elastic stress analyses were performed with a commercially available finite element code. Secondary orientation of the single-crystal superalloy was offset with respect to the global coordinate system in increments from 0° to 90° and stresses developed within the single crystal were determined for each loading condition. The results indicated that the stresses were strongly influenced by the angular offset between the secondary crystal orientation and the global coordinate system. The degree of influence was found to vary with the type of loading condition (mechanical, thermal, or combined) imposed on the single-crystal superalloy.

17. Key Words (Suggested by Author(s))

Single crystal
Secondary
Orientation
Elastic behavior

18. Distribution Statement

Unclassified – Unlimited
Subject Category 39

19. Security Classif. (of this report)	20. Security Classif. (of this page)	21. No. of pages	22. Price*
Unclassified	Unclassified	12	A03

NASA FORM 1626 OCT 86

*For sale by the National Technical Information Service, Springfield, Virginia 22161